The Dependence of EM Energy Absorption Upon Human Head Modeling at 900 MHz

Volker Hombach, *Member, IEEE*, Klaus Meier, Michael Burkhardt, Eberhard Kühn, *Member, IEEE*, and Niels Kuster

Abstract— **In this paper the dependence of electromagnetic energy absorption at 900 MHz in the human head on its anatomy and its modeling are investigated for RF-sources operating in the very close proximity of the head. Different numerical head phantoms based on MRI scans of three different adults were used with voxel sizes down to 1 mm^3. Simulations of the absorption were performed by distinguishing the electrical properties of up to 13 tissue types. In addition simulations with modified electric parameters and reduced degrees of complexity were performed. Thus, the phantoms greatly differ from each other in terms of shape, size, and internal anatomy. The numerical results are compared with those of measurements in a multitissue phantom and two homogeneous phantoms of different shapes and sizes. The results demonstrate that size and shape are of minor importance. Although local SAR values depend significantly on local inhomogeneities and electric properties, the volume-averaged spatial peak SAR obtained with the homogeneous phantoms only slightly overestimates that of the worst-case exposure in the inhomogeneous phantoms.**

I. Introduction

In the past few years there has been an increase in public concern about possible health risks from the electromagnetic (EM) energy emitted by handheld mobile telecommunications equipment (MTE). The first step necessary for an assessment of the potential risks is to analyze and quantify the EM field induced in the various tissues of the human head caused by the use of a handheld cellular phone.

Two kinds of dosimetric assessments are of special interest, depending on the emphasis placed on the assessment's endpoint. Detailed information on the distribution of the induced electric and magnetic field strengths inside the various tissues of the head is a prerequisite to designing and performing the most meaningful biological experiments. On the other hand, an efficient, accurate, and reliable assessment is needed to implement a standardized compliance test for MTE with the basic safety limits.

To analyze the possible range of variations of the induced field strengths in the various tissues requires an extensive effort, since the local field strengths strongly depend on a large number of parameters, such as:

1) operational frequency and antenna input power;
2) position of the device with respect to the head;
3) design of the device;
4) the outer shape of the head;
5) the distribution of the different tissues within the head; and
6) the electric properties of these tissues.

The last three factors are different for various individuals and can even change with time. For example, the outer shape depends on the individual profile and on any movement of the mouth or the eyes. The electric parameters of a human body vary with levels of physical and metabolic activity, health, and age. The variations in all these properties lead to a spread in the analyzed absorption distribution. A strategy on how to obtain scientifically valuable information from this large parameter range has not been worked out yet. However, it is clear that such an approach would not be suited for a type-approval procedure, which should be time-efficient, cost-effective, and of utmost reliability. Simplifications are therefore required.

The current basic safety limits applicable for mobile communications equipment are defined in terms of the specific absorption rate (SAR). Three different limits are defined: 1) a whole-body average SAR; 2) a local peak SAR; and 3) a specific absorption (SA), which limits the power of short pulses. 1) and 2) must be averaged over a defined period of time. In the case of an MTE operating at frequencies above 300 MHz, the absorption affects only those parts of the body which are close to the device. Hence, the most critical value is the local peak SAR limit. In Europe the basic limit set for the general public is 2 mW/g averaged over a volume equivalent to 10 g and a period of 6 min. [1]. The ANSI/IEEE standard [2] defines a stricter limit for an uncontrolled environment of 1.6 mW/g averaged over a volume of 1 g and a period of 30 min.

The objective of a type-approval procedure is therefore to assess the maximum spatial peak SAR which the specific device under test would induce among all users under various operational positions. The currently most often used system for testing MTE is the measurement setup using a homogeneous anatomically-shaped phantom filled with a liquid simulating brain tissue [3], [4]. The rationale behind this approach comes from the energy absorption mechanism in the close near field of antennas [5], which concludes that the most determining parameters for volume-averaged values are the time-averaged antenna input power, operational frequency, design of the device, and its position with respect to the head, and to a much lesser extent, on the physical properties of the head.

In this paper the effects of head properties, such as size, shape, and inhomogeneities on the absorption are studied to

Manuscript received October 2, 1995; revised May 16, 1996. This work was supported in part by DeTeMobil GmbH and Swiss Telecom PTT.

V. Hombach and E. Kühn are with Deutsche Telekom, Technologiezentrum, 64 276 Darmstadt, Germany

K. Meier, M. Burkhardt, and N. Kuster are with the Swiss Federal Institute of Technology Zurich, 8096 Zurich, Switzerland.

Publisher Item Identifier S 0018-9480(96)07032-9.

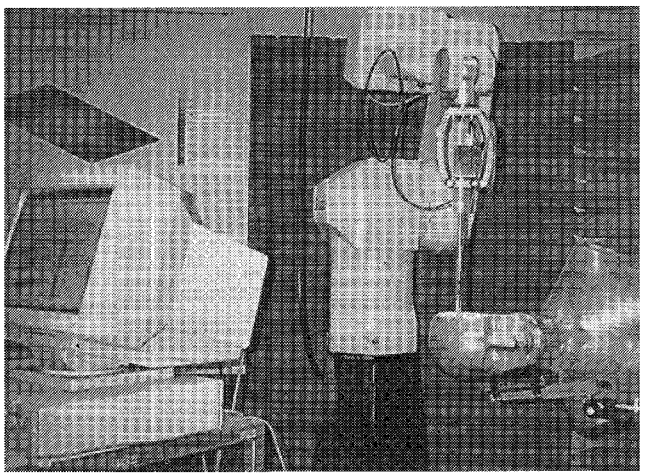

Fig. 1. Experimental setup: Dosimetric Assessment System DASY 2.0 is used during the experimental phase of this investigation. A six axis, high-precision robot positions the E-field probe inside the phantom head models.

evaluate the applicability of homogeneous head phantoms for compliance tests.

II. Numerical and Experimental Techniques

A. Simulation Technique

In electrodynamics by far the most flexible way to investigate effects which depend on multiple parameters is with computer simulations, since geometry and domain properties can be easily varied. Many numerical techniques exist for the analysis of complex near-field scattering problems, whereby the finite-difference time-domain (FDTD) technique [6] has proven to be the most efficient method for studying absorption in strongly inhomogeneous bodies. FDTD is currently used by various groups to study the absorption in the human head from mobile phones (e.g., [7]–[10]) and to test novel antenna designs (e.g., [11], [12]).

The applied, commercially available code MAFIA [13] is based on the finite integration technique (FIT), which is well described in [14]. This technique is conceptually slightly different than FDTD but leads to the same numerical scheme. The open domain is bounded by second-order Mur absorbing boundary conditions. Excitation is done by a smoothly-increasing harmonic function and the computation is terminated after steady state is reached (usually after 10 to 20 periods). Computational time for 2.5 million voxels was typically three hours on an IBM RS6000/560 computer.

B. Experimental Technique

The setup shown in Fig. 1 was used to perform the experimental studies. The SAR distribution is determined by measuring the electric field with miniaturized E-Field probes inside shell phantoms filled with tissue simulating liquids. The probes are positioned by a six-axis precision robot (Stäubli RX90) with a position repeatability of better than ± 0.02 mm (at constant temperature). An optical surface-detecting system is integrated into the probes, which enables the accurate positioning of the probe with respect to the phantom's inner surface. The SAR distribution can be measured for basically any volume. For dosimetric assessments of RF-sources close to the head, the following measurement strategy has been implemented: The E-field probe first scans over a large area inside the head to roughly localize the maximal SAR value. In a subsequent step SAR-measurements are done along a fine grid within a 35 g volume cubically shaped around this maximal value. This cube is large enough to provide enough data to evaluate the spatial peak SAR. The whole procedure is completely automated and takes less then 15 min. A detailed description of the system is given in [4]. An error analysis has

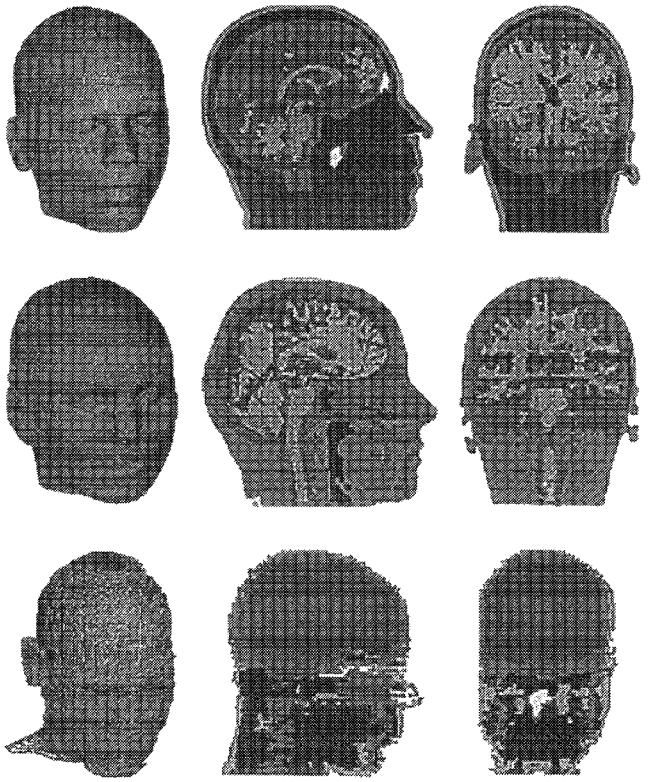

Fig. 2. Surface view and two cross-sectional views of the three MRI phantoms.

TABLE I
Three Different Head Models for Computer Simulations

	M1 ref. [17]	M2 ref. [18]	M3 ref. [8]
Head Volume	4.44 dm^3	3.35 dm^3	4.26 dm^3
Tissues	13	120	12
Computational Space	175×230 ×226 mm	159×208 ×201 mm	159×206 ×249 mm
Voxel Size	(1 mm)^3	(1.075 mm)^3	(1.875 mm)^2 ×3 mm

TABLE II
TISSUE PARAMETERS FOR THE FIT SIMULATIONS

Tissue	ref. [16] ϵ_r	ref. [16] σ [mho/m]	ref. [10] ρ [kg/m^3]
bone (M1, M2, M3, M4)	20.9	0.33	1850
cartilage (M1, M2, M3)	41.9	0.83	1000
skin (M1, M2, M3, M4)	40.7	0.65	1100
fat (M1, M2, M3)	10.0	0.17	1100
muscle (M1, M2, M3, M4)	57.4	0.82	1040
brain, grey matter (M1, M2)	53.8	1.17	1030
brain, white matter (M1, M2)	34.5	0.59	1030
brain, average (M3, M4)	41.0	0.86	1030
CSF (M1, M2, M3)	79.1	2.14	1000
eye humour (M1, M2, M3, M4)	67.9	1.68	1010
eye lens nucleus (M1, M2, M3)	36.6	0.51	1050
eye lens outer (M1, M2, M3)	51.6	0.90	1050
eye sclera (M1, M2, M3)	54.9	1.17	1020
blood (M3)	55.0	1.86	n/a
parotid gland (M3)	70.0	1.90	n/a

TABLE III
TISSUE PARAMETERS FOR THE EXPERIMENTAL SIMULATIONS

Tissue	ref. [16] ϵ_r	ref. [16] σ [mho/m]	ref. [10] ρ [kg/m^3]
bone (E1, M4)	14.8	0.15	1850
skin (E1, M4)	42.0	0.78	1100
muscle (E1, M4)	51.7	1.11	1040
brain, average (E1, M4, E2, E3)	41.0	0.88	1030
eye	67.9	1.68	1030

Fig. 3. Photo of the experimental head phantom E1. Five tissues are simulated: brain, bone, skull, muscle, and skin.

shown that the uncertainty of the measured spatial peak SAR values is less than 20%, using the probe calibration technique as described in [15].

III. HEAD PHANTOMS

A. Exposure

In order to avoid the uncertainties of modeling actual handsets, a dipole 0.45λ in length was chosen. It was positioned

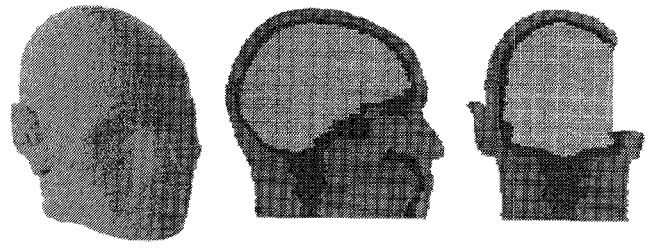

Fig. 4. Numerical phantom which corresponds to the experimental head phantom E1. Five different tissues are distinguished: brain, bone, skull, muscle, and skin.

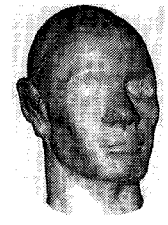

Fig. 5. Polyester copy E2 of phantom E1.

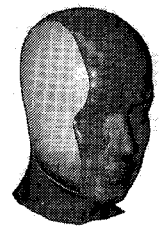

Fig. 6. Fiberglass head-torso phantom E3 which is used for dosimetric tests of mobile telephones.

at a distance of 15 mm from the head and with an orientation parallel to the body's axis (see figures).

In the numerical approach the dipole was simulated as a filament 0.45λ in length. A SPEAG 900 MHz test dipole of exactly the same length and made of standard 3.6 mm semirigid coaxial cable was used for the measurements. The bifilar matching line had a length of exactly $\lambda/4$ at 900 MHz, allowing direct measurement of the feedpoint impedance of the dipole, using a network analyzer with a shorted feeding gap as reference. Accurate information about the feed point impedance which changes considerably with distance from the body is essential, since the absorption is not primarily proportional to the output power but to the square of the antenna current [5]. In order to compare the results, all values were therefore normalized to an antenna current of 100 mA.

B. Numerical Phantoms

Accurate phantoms of heterogeneous human heads can be generated on the basis of magnetic resonance imaging (MRI). The translation of the three-dimensional (3-D) data sets of relaxation times into the tissue distribution is a difficult task and generally requires a person trained either in medicine or biology, who is able to distinguish both transitional and marginal regions. MRI produced in different laboratories, by different scientists and from different test subjects inevitably contain differing discretizations.

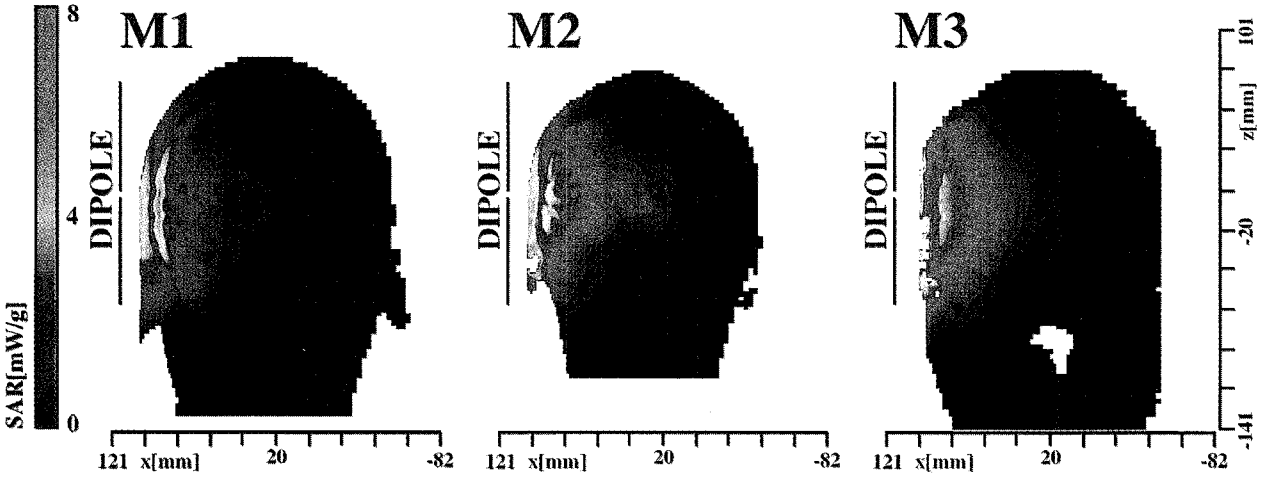

Fig. 7. SAR distribution in the xz plane of head phantom M1 (left), M2 (middle), and M3 (right).

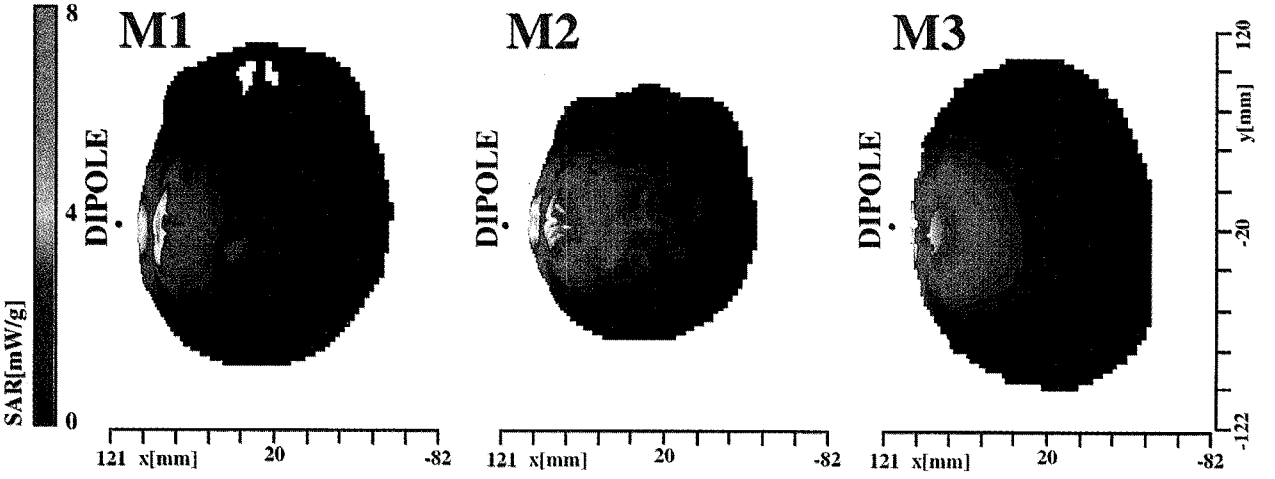

Fig. 8. SAR distribution in the xy plane of head phantom M1 (left), M2 (middle), and M3 (right).

In this study three phantoms discretized by different groups, based on MRI data sets of three different adults are used and their results compared. Fig. 2 shows the outer shapes and two cross-sectional views of these head phantoms and Table I gives the data of discretization. The ear closest to the antenna needs special attention:

During normal use of a hand-held telephone, the ear is pressed against the head and, therefore, changes its shape. In order to avoid effects caused by the different ear modeling, which may mask the effects of the head itself, the outer right ear of the head phantoms was removed.

The phantoms can be described as follows:

1) Model M1 was taken with the highest resolution. Its voxel size is 1 mm in all three cartesian dimensions. M1 has the largest volume. The brain region was segmented very carefully. For the entire head 13 tissue types were simulated. However, the lower part of the head was assigned to only one tissue type.
2) The second head phantom M2 has nearly the same voxel size. It was developed for the training of medical students and distinguishes among 120 tissue types. For the EM analysis this large number needed to be reduced to 13 different tissues for which electric parameters are available [16].
3) The third head phantom M3 was taken with a voxel size of about 12 mm^3. The discretization is relatively crude. In the original MRI model the skin was not identified. In the computer model the skin was added as an outer layer with a thickness of one voxel. The brain region of head phantom M3 is homogeneous and assigned only one tissue type.
4) The fourth numerical phantom M4 (see Fig. 4) corresponds to the experimental phantom E1 described below (Fig. 3). It was derived from MR and CT cross sections taken every 2 mm. The voxel size was 2 mm $\times$ 2 mm $\times$ 2 mm.

Comparing the data of different publications reveals a spread in the values given for the electric parameters of different types of tissue. Table II shows the electric parameters we have chosen for this study. The permittivity and the conductivity

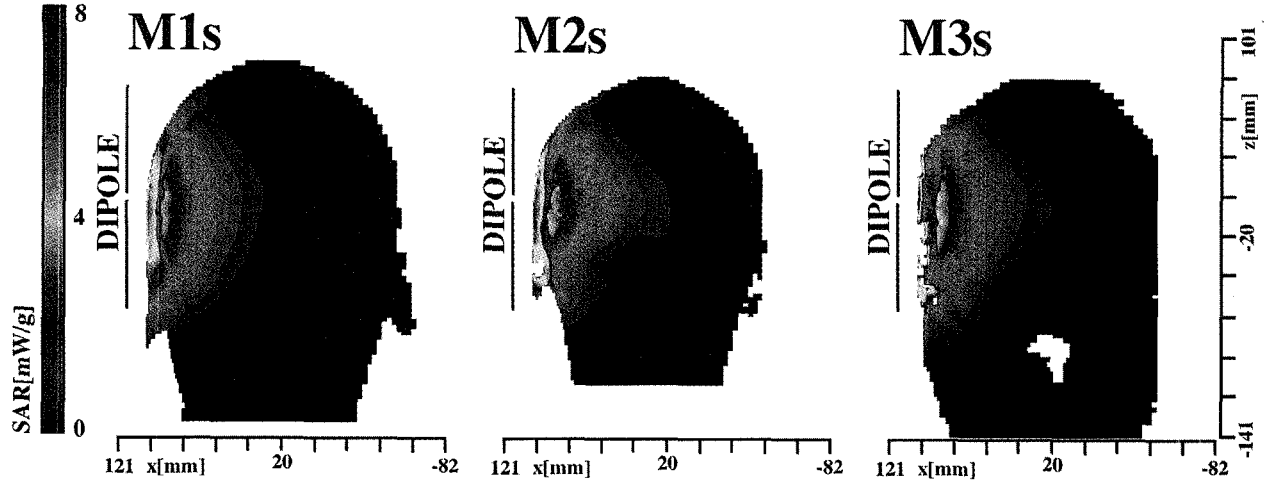

Fig. 9. SAR distribution in the xz plane of head phantom M1s (left), M2s (middle), and M3s (right).

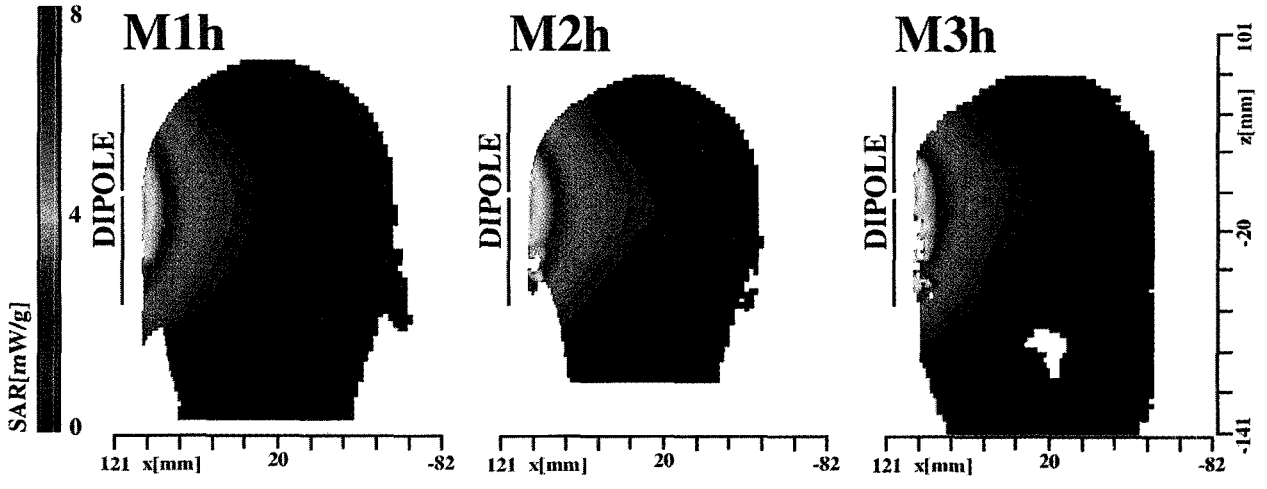

Fig. 10. SAR distribution in the xz plane of head phantom M1h (left), M2h (middle), and M3h (right).

of the tissues of phantoms were taken from the dielectric database [16]. Since M3 did not distinguish between different brain tissues, an averaged value of white and gray matter for brain tissue was used. In order to better compare the results from the numerical phantoms with those from the experimental phantoms, M4 was simulated with the tissue properties of Table II, as well as with those of Table III.

With numerical simulations, using FIT or other finite-difference codes, it is easy to attribute different tissue parameters to different mesh cells. However, the tissue discretization and the assignment of the electrical parameters to various tissues is fraught with considerable uncertainties. Therefore, the question of whether these parameters significantly alter the absorption has been studied by relating different parameters to the various tissues:

1) anatomically correct head phantoms with tissue distributions derived from MRI (referred to as M1, M2, M3, M4);
2) simplified head phantoms, which have the outer shape of the MRI phantoms, but which contain only one tissue with high water content ($\epsilon_r = 43.5$, $\sigma = 0.9$ mho/m) and one with low water content, using the parameter of bone tissue, i.e., $\epsilon_r = 21$, $\sigma = 0.33$ mho/m (referred to as M1s, M2s, M3s, M4s); and
3) homogeneous head phantoms with the outer shape of the MRI phantoms which contain only one tissue type with $\epsilon_r = 43.5$, $\sigma = 0.9$ mho/m (referred to as M1h, M2h, M3h, M4h).

C. Experimental Phantoms

Three different phantoms were studied.

1) *Complex, Five Tissue Model* referred to as E1: artificial "*in-vivo*" phantom head from Microwave Consultants (Fig. 3). The phantom head simulates four tissue types: skull, muscle, skin and eyes. The fifth tissue, brain, is simulated by a sugar-water-salt solution with the electric parameters of the mean value between gray and white matter ($\epsilon_r = 41$, $\sigma = 0.88$ mho/m). The parameters of the other tissues are given in Table III. The head size

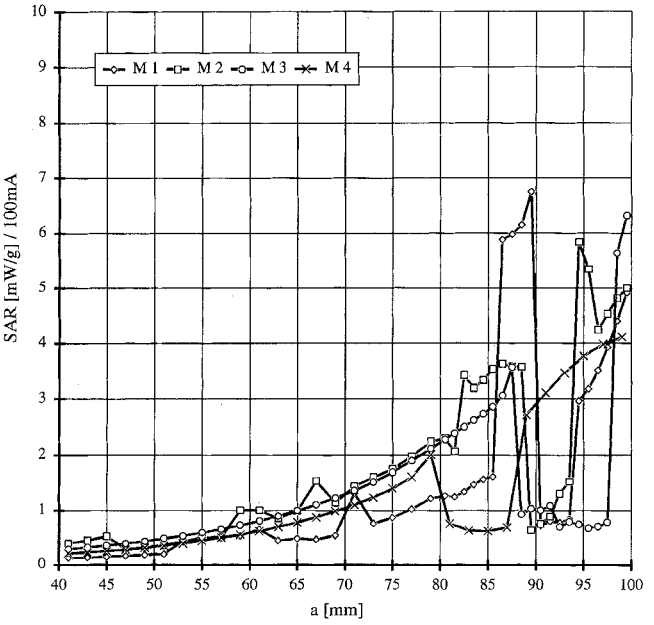

Fig. 11. SAR profile on the x axis through the complex head phantoms.

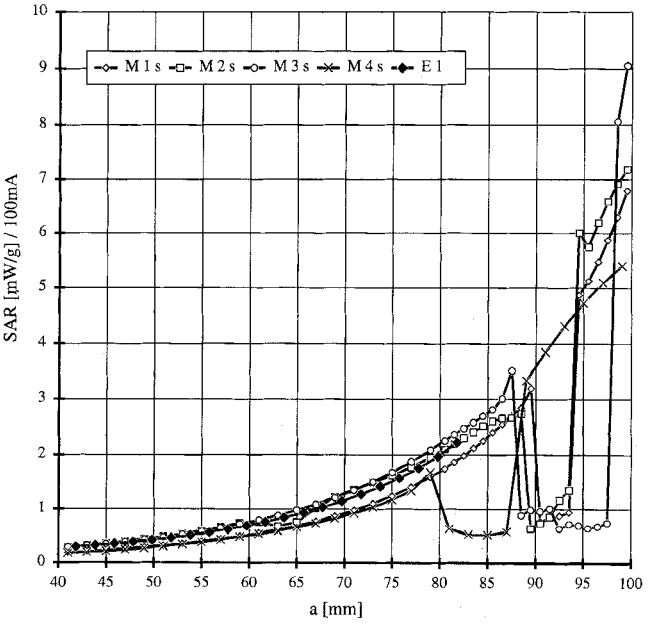

Fig. 12. SAR profile on the x axis through the simplified head phantoms.

does not correspond to that of an average person since the volume of the brain is only about 1 liter instead of the typical value amounting to about 1.4 to 1.5 liters. In addition the skin-skull layer in the area above the ear is wider (15.5 mm) than for an average person.

2) *Homogeneous Shell Copy* referred to as E2: exact copy of the outer shape of the previous complex phantom (Fig. 5). The shell is made of polyester ($\epsilon_r = 4$) and the thickness varies between 3 mm and 6 mm due to the manufactoring process. This phantom is again filled with the same brain tissue simulating liquid. About 2.5 liters can be used. In this case not only the brain area but the entire human head is modeled homogeneously.

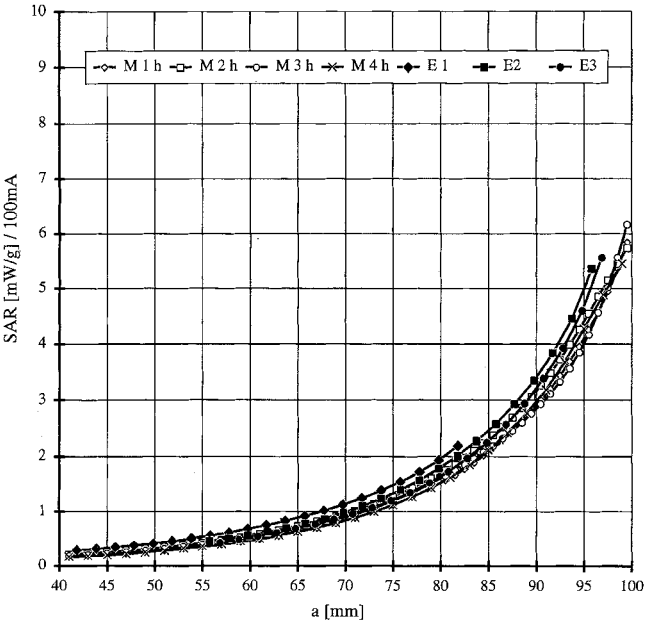

Fig. 13. SAR profile on the x axis through the homogeneous head phantoms.

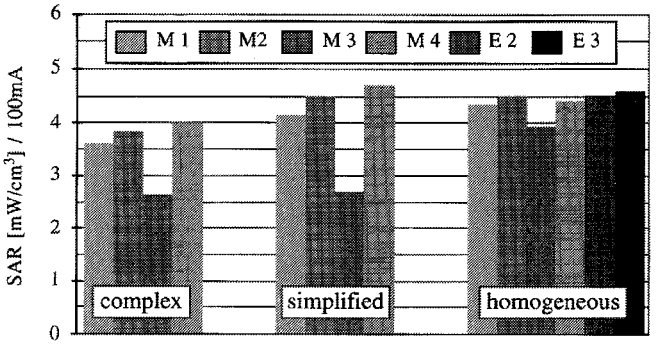

Fig. 14. Peak SAR averaged over 1 g of tissue mass.

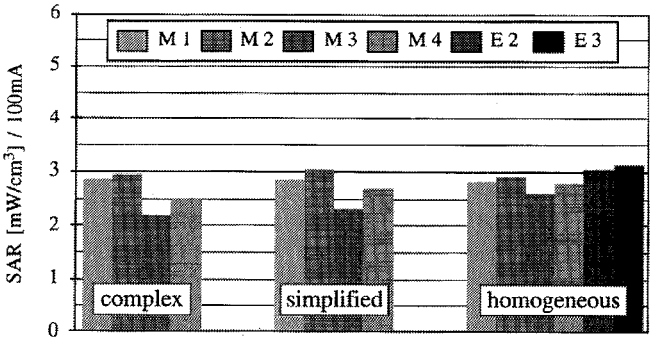

Fig. 15. Peak SAR averaged over 10 g of tissue mass.

3) *Homogeneous Torso Model* referred to as E3: head-torso phantom of a human being (Fig. 6). The shell is anatomically correctly shaped and is made of a 3 mm thick fiberglass ($\epsilon_r = 2.8$). Shape and size of this phantom are very different from the shell copy of the complex phantom. It is considerably larger (4 liters instead of 2.5). For dosimetric characterizations of MTE this phantom is currently used in several laboratories in Europe and the United States.

TABLE IV
ANTENNA CURRENT, ANTENNA INPUT POWER, AND RATIO OF ABSORBED POWER TO INPUT POWER OF VARIOUS HEAD PHANTOMS

phantom	I_{rms} [mA]	P_{in} [W]	P_a/P_{in}
anatom. corr.			
M1	100	0.44	0.72
M2	100	0.48	0 69
M3	100	0.52	0.69
simplified			
M1s	100	0.43	0.74
M2s	100	0.46	0.69
M3s	100	0.51	0.70
homogeneous			
M1h	100	0.41	0.72
M2h	100	0.41	0.65
M3h	100	0.41	0.70
E2	100	0.45	-
E3	100	0.46	-

IV. RESULTS

A. SAR Distribution in Various Head Phantoms

The coordinate system used for analysis and presentation of the results is oriented so that the z axis is parallel to the head axis and the dipole axis. The x axis runs from the body axis toward the dipole feedpoint. The dipole feedpoint is always located at $x = 115$ mm, $y = 0$, $z = 0$.

Figs. 7 and 8 show the qualitative SAR distribution of each of the anatomically correct head phantoms, in both the xz plane and the xy plane, respectively. The dipole is seen as a line or a point. High SAR values are in red, low SAR values in blue. The results can be summarized as follows:

1) The region with high absorption values in all head phantoms is small and close to the feedpoint of the dipole. In most parts of the head the EM field is relatively low.
2) Two SAR maxima can be identified in each of the MRI based phantoms, one on the skin's surface and one on the brain's surface. The SAR induced in bone tissue is considerably lower. The absolute values of the maxima differ from model to model.
3) Examining the details of the SAR distribution in the brain region, one can identify varying SAR distributions in phantoms M1 and M2, which may be attributed to different conductivities of gray and white matter. Phantom M3 reveals a monotonic decay of the absorption rate inside the brain tissue.

Fig. 9 depicts the simplified head phantoms with only two types of tissue. The resulting SAR distribution shows some agreement and differences with respect to that of the anatomically correct phantoms.

1) The simplified phantoms also exhibit the two SAR maxima at the skin surface and the brain surface with the minimum in the bone in between. The maxima at the brain surface in Fig. 9 are lower than those in Fig. 7. This is primarily due to the higher conductivity ($\sigma = 0.9$ mho/m) which is used for the skin in the simplified phantoms in comparison to the actual skin conductivity of 0.65 mho/m.
2) Since no tissues are distinguished inside the brain region, the SAR distribution shows a smooth decay.

Fig. 10 shows the SAR distributions inside the homogeneous head phantoms M1h, M2h, and M3h. These differ from those of the anatomically correct and simplified phantoms as follows:

1) Only one SAR maximum is observed at the phantom surface.
2) Inside the phantom the EM field decays monotonically.

All these differences can be directly explained by the energy absorption mechanism. According to [5], the induced SAR is primarily determined by the square of the H-field which drops inversely proportional to the square of the distance from the source. In the case of transmitters very close to the head, this factor is dominant so that even lossy bone tissue can be approximated by a layer of air of the same thickness in order to assess the SAR in the brain tissue behind this layer. In other words, the distance dependence dominates the field attenuation due to absorption. The often discussed effects occurring in far field exposure situations (e.g., refraction effects, etc.) are negligible in case of the extreme near field exposure. Quantitative presentations of the SAR values in Figs. 11 to 13 on the x axis in the range 40 mm $\leq x \leq$ 100 mm confirm this. The head surface facing the dipole is located at $x = 100$ mm. In addition, in the same figures the simulations are compared with the measurement data which are normalized to an antenna feedpoint current of 100 mA. Noticeable is the good agreement between measured and simulated data.

B. Averaged SAR Values

The volume-averaged spatial peak SAR values (mW/cm^3) were derived by shifting a cube of 10 mm (1 g) or 21.5 mm side length (10 g) over the head region, calculating $\sigma|E|^2$ averaged over each cube and searching for the position where this value is at a maximum.

The averaged values for the experimental phantoms are derived as described earlier. 175 measurements inside a cube of about 35 g of brain tissue provided sufficient data to accurately locate the spatial peak SAR values averaged over 1 g and 10 g using interpolation and extrapolation routines.

This is a departure from the definition in the standard requiring averaging over volume of 1 g or 10 g tissue, but is much easier to compute and to compare. It, however, slightly underestimates the mass-averaged SAR values.

In Figs. 14 and 15 SAR values averaged over 1 cm^3 and 10 cm^3 for the various heads and different modelings are compared. The difference between the various heads and the different modelings are surprisingly small. The smaller values of phantom M3 can be explained by the thickness of the bone layer which exceeds that of an average adult. The

homogeneous head overestimates the absorption compared to the highest value found among the inhomogeneous phantoms by 25% for the 1 cm^3-average and by only 10% for the 10 cm^3-average.

In Table IV the antenna input power P_{in} as well as the ratio of absorbed P_a to the antenna input power are given. The radiated power is about 450 mW and varies by 20% depending on the modeling. Typically, 70% of the antenna input power is absorbed by the head. The variation of <15% indicates that homogeneous heads are suitable for the purpose of radiation optimization of MTE.

V. Conclusion

The results basically confirm the conclusions of [5] that the spatial peak SAR is scarcely affected by the size and the shape of the human head for electromagnetic sources at a defined distance from the human head. Compared to other factors, such as distance of the source from the head and design of the devices, the effects caused by the complex anatomy are minor especially in the case of volume-averaged values. Due to the strong radial decay of the H-field in the vicinity of the source, variations of the bone conductivity have scarcely any effect on the absorption in the brain tissue.

The comparison of the results obtained from the inhomogeneous and homogeneous phantoms suggests that homogeneous phantoms are highly suited to be used in compliance tests for handheld MTE operating in the 900 MHz band. The overestimation of the averaged spatial peak SAR values is small when compared to the largest value obtained by the inhomogeneous phantoms. This is especially true if the values are averaged over a volume equivalent to 10 g. The major advantage of using simple homogeneous phantoms is that the number of tests can be reduced since small shifts of the source parallel to the surface result in almost no changes in the spatial peak SAR values. In case of inhomogeneous modeling variations of several dB must be expected for shifts of a few millimeters. Therefore inhomogeneous phantoms might result in artificially low SAR values for some positions of the device with respect to the head, which would not represent the actual exposure of the various users.

These results were found for sources operating at 900 MHz but can be extended for frequencies down to 300 MHz. Whether they are valid for the 1.5 to 2 GHz band must be subject of further study.

Acknowledgment

The authors gratefully acknowledge the advice of F. Lauer and B. Eicher and the help of T. Schwitter.

References

[1] CENELEC CLC/SC111B, *European Prestandard (prENV 50166-2, Human Exposure to Electromagnetic Fields High-Frequency: 10 kHz–300 GHz*, CENELEC, Brussels, Jan. 1995.

[2] ANSI, *ANSI/IEEE C95.1-1992: IEEE Standard for Safety Levels With Respect to Human Exposure to Radio Frequency Electromagnetic Fields, 3 kHz to 300 GHz.* New York: IEEE, 1992.

[3] Q. Balzano, O. Garay, and T. J. Manning, "Electromagnetic energy exposure of simulated users of portable cellular telephones," *IEEE Trans. Veh. Technol.*, vol. 44, no. 3, pp. 390–403, Aug. 1995.

[4] T. Schmid, O. Egger, and N. Kuster, "Automated E-field scanning system for dosimetric assessments," *IEEE Trans. Microwave Theory Tech.*, vol. 44, no. 1, pp. 105–113, Jan. 1996.

[5] N. Kuster and Q. Balzano, "Energy absorption mechanism by biological bodies in the near field of dipole antennas above 300 MHz," *IEEE Trans. Veh. Technol.*, vol. 41, no. 1, pp. 17–23, Feb. 1992.

[6] A. Taflove, *Computional Electrodynamics: The Finite-Difference Time-Domain Method.* Norwood, MA: Artech House, 1995.

[7] P. J. Dimbylow and S. M. Mann, "SAR calculations in an anatomically realistic model of the head for mobile communication transceivers at 900 MHz 1.8 GHz," *Phys. Med. Biol.*, vol. 39, no. 12, pp. 1537–1553, 1994.

[8] O. P. Gandhi, J. Y. Chen, and D. Wu, "Electromagnetic absorption in the human head for mobile telephones at 835 MHz and 1900 MHz," *Int. Symp. Electromag. Compat.*, Roma, 1994, pp. 1–5.

[9] L. Martens, J. De Moerloose, and D. De Zutter, "Calculation of the electromagnetic fields induced in the head of an operator of a cordless telephone," *Radio Sci.*, vol. 30, no. 1, pp. 283–290, Jan. 1995.

[10] M. A. Jensen and Y. Rahmat-Samii, "EM interaction of handset antennas and a human in personal communications," *Proc. IEEE*, vol. 83, no. 1, pp. 7–17, Jan. 1995.

[11] G. F. Pedersen and J. B. Andersen, "Integrated antennas for handheld telephones with low absorption," in *44th IEEE Veh. Technol. Conf.* , Stockholm, Sweden, June 1994, pp. 1537–1541.

[12] J. Fuhl, P. Nowak, and E. Bonek, "Improved internal antenna for hand-held terminals," *Electron. Lett.*, vol. 30, no. 22, pp. 1816–1818, 1994.

[13] CST, *The MAFIA Collaboration, User's Guide Mafia Version 3.x*, CST GmbH, Lautenschlaegerstr. 38, D 64289 Darmstadt, Germany, 1994.

[14] T. Weiland, "Maxwell's grid equations," *Frequenz*, vol. 44, no. 1, pp. 9–16, 1990.

[15] K. Meier, M. Burkhardt, T. Schmid, and N. Kuster, "Broadband calibration of E-field probes in lossy media," submitted for publication in *IEEE Trans. Microwave Theory Tech.*, 1996.

[16] Microwave Consultants, *Dielectric Database*, Microwave Consultants Ltd., London, pp. 1–5, 1994.

[17] G. Bielke and S. Meindl, "Dreidimensionale segmentierte MR-Bilddatensätze," Tech. Rep. Nr. 6564/33038, Deutsche Klinik für Diagnostik e. V., Forschungsvertrag DBP Telekom, 1993.

[18] K. H. Höhne, M. Bomans, M. Reimer, R. Schubert, U. Tiede, and W. Lierse, "A volume-based anatomical atlas," *IEEE Computer Graphics Applicat.*, pp. 72–77, 1992.

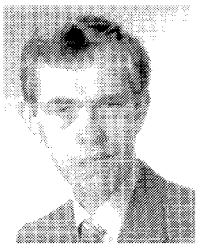

Volker Hombach (M'76) received the Dipl.-Ing. degree in electrical engineering from RWTH Aachen, Germany, and the Dr.-Ing. from the Ruhr-Universität Bochum, Germany, in 1975 and 1981, respectively.

Since 1981 he has been with the Forschungszentrum of Deutsche Telekom in Darmstadt, Germany. He has been involved in the research of diffraction effects and the design and optimization of reflector antennas and feeds. His current interests include electromagnetic scattering and absorption, electromagnetic compatibility, and electromagnetic radiation hazard protection.

Dr. Hombach is a member of the German Society in Information Technology (ITG). He received the ITG Award in 1989.

Klaus Meier was born in Austria in March 1965. He received the Diploma degree in electrical engineering from the Swiss Federal Institute of Technology (ETH) Zurich in 1991.

He joined the Institute for Field Theory and Microwave Electronics at the ETH in 1991. Since 1992 he has been involved in the development of the dosimetric assessment system DASY. He is currently finishing the Ph.D. on the development of a phantom for standardized compliance tests of mobile telecommunication equipment. He is a cofounder of the spin-off company Schmid & Partner Engineering AG.

Michael Burkhardt was born in Germany in March 1969. He received the Diploma in electrical engineering from the Technische Hochschule Darmstadt in 1995 with emphasis on computational electrodynamics. In 1993 he conducted his semester work at the Institut National Polytechnique de Grenoble (INPG), France.

In May 1995 he joined the Institute of Field Theory and Microwave Electronics, ETH, where he is involved in the development of a modular platform for electromagnetic simulations. In addition he has performed various studies using time and frequency domain techniques.

Eberhard Kühn (M'84) was born in Berlin, Germany, in 1938. He received the Dipl.-Ing. and Dr.-Ing. degrees in electrical engineering from the Technical University of Braunschweig, Germany, in 1966 and 1972, respectively.

From 1972 to 1977 he worked as a Research Engineer at the Deutsche Bundespost Research Institute in Darmstadt, Germany. Between 1977 and 1994 he was Head of the Antenna and Wave Propagation Division of the same institution. Since 1994 he has been Head of the Radio Communications Division of the Deutsche Telekom's Technology Center in Darmstadt, Germany. His research interests include radio communications, computational electromagnetics, and bioelectromagnetics.

Dr. Kühn is a member of the German Society in Information Technology (ITG, formerly NTG). He received the NTG Award in 1975 and the Microwave Prize (with two coauthors) of the 14th European Microwave Conference, Liege, Belgium, in 1984. From 1975 to 1990 he was Associate Editor of *NTZ-Archiv*, the former scientific journal of the ITG.

Niels Kuster was born in Olten, Switzerland in June 1957. He received the Diploma and Ph.D. degrees in electrical engineering from the Swiss Federal Institute of Technology (ETH) in Zurich.

He joined the Electromagnetics Laboratory at ETH in 1985 where he was involved in the research and development of the generalized multipole technique (GMT) and the 3-D MMP code. In 1992 he was Invited Professor at Motorola Inc. in Fort Lauderdale, FL for a trimester. He currently is Assistant Professor at the Department of Electrical Engineering, ETH Zurich. His research interests include all aspects of numerical methods in electrodynamics, antenna design and bioelectromagnetics.

Dr. Kuster is a member of various scientific societies and official member of URSI Commission K.